Supporting Information

A comprehensive approach for the Characterization of Porous Polymers by ^{13}C and ^{15}N Dynamic Nuclear Polarization NMR Spectroscopy

Sven Grätz[a†], Marcos de Olivera Junior[b,c†], Torsten Gutmann[b]*, Lars Borchardt[a]*

Table of contents

1 General Methods

Infrared spectroscopy (IR) was carried out with an IR-spectrometer Bruker Vertex 70 with a Specac Golden Gate ATR unit. The spectra were treated with ATR-correction by the OPUS 6.5 software.

Nitrogen physisorption measurements were performed at 77 K on an Autosorb-IQ-C-XR and Quadrasorb (Quantachrome Instruments). High purity gases were used for physisorption measurements (N_2: 99.999%). Specific surface areas (SSABET) were calculated applying the model of Brunauer, Emmet and Teller (BET) in a relative pressure range that fits to the consistency criteria proposed by Rouquerol and Llewellyn.[1] Pore size distributions were calculated using the Quenched Solid Density Functional Theory (QSDFT) method for carbon (slit pores, equilibrium kernel) on the adsorption branch.

We utilized the QSDFT kernel for carbon materials, which is not perfectly suited for polymers. However, this is common practice since alternatives are not available yet.

Scanning electron microscopy (SEM) images were obtained using a Hitachi SU8020 SEM equipped with a secondary electron (SE) detector. Prior to the measurement the samples were prepared on an adhesive carbon pad and sputtered with gold to obtain the necessary electron conductivity.

2 Samples for DNP NMR experiments

The polymers were washed thoroughly and dried over vacuum before loading them for the DNP NMR experiments. Samples were prepared for DNP NMR measurements by mixing ca. 10 mg of the appropriate sample with ca. 20 µL of the polarizing agent solution. The mixture was prepared inside the MAS rotor used for the experiments. It was centrifuged for 2 minutes to ensure homogeneous impregnation of the solution through the sample. The solution consisted of 15 mM of an appropriate organic radical in an organic solvent. The organic solvents were either 1,1,2,2-tetrachloroethane (TCE) or dimethylsulfoxide (DMSO). The organic radicals were: TEMPO (Sigma Aldrich), TEKPol (Cortecnet, France),[2] AMUPol (Cortecnet, France),[3] BDPA (S. Th. Sigurdsson, Iceland)[4] and bTbK (O. Ouari, Aix-Marseille University)[5]. The solvent/radical combinations employed in this work, and the respective enhancements observed in DNP enhanced $^{13}C\{^1H\}$ CP MAS experiments on sample PP-1 are given in Table S1.

Table S1: Solvent/radical combinations employed for DNP sample preparations of PP-1 and the respective enhancements observed in DNP enhanced $^{13}C\{^1H\}$ CP MAS experiments

DNP-Matrix	Enhancement
TCE+TEKPol	3 ± 1
TCE+TEMPO	[a]
TCE+BDPA	2.0 ± 0.5
TCE+bTbK	7 ± 1
DMSO+bTbK	[a]
DMSO+AMUPol	[a]

[a] **Enhancement could not be estimated. The signal intensity variation due to sample heating under mw irradiation is domin**ant.

3 Characterization Data

The polymers were synthesized accroding to the literature.[6–9]

3.1 Textural Data for the different polymers

Table S2: Textural data of the used porous polymers

Sample	Surface Area[a] $m^2 \cdot g^{-1}$	Pore Volume[b] $cm^3 \cdot g^{-1}$	Pore width[c] nm	Elemental Composition
PP-1[6]	740	0.40	0.90, 1.56, 3.20	C, N, H
PP-2[9]	1850	0.95	0.90, 1.56, 3.20	C, S, H
PP-3[7]	670	0.53	1.05, 2.43, 4.84	C, H
PP-4[8]	1550	1.12	0.66, 0.96, 3.10	C, H

[a] according to N_2 isotherms by the Brunauer-Emmett-Teller theory, utilizing the Rouquerol method

[b] determined at $p/p_0 = 0.9$

[c] determined by DFT calculations

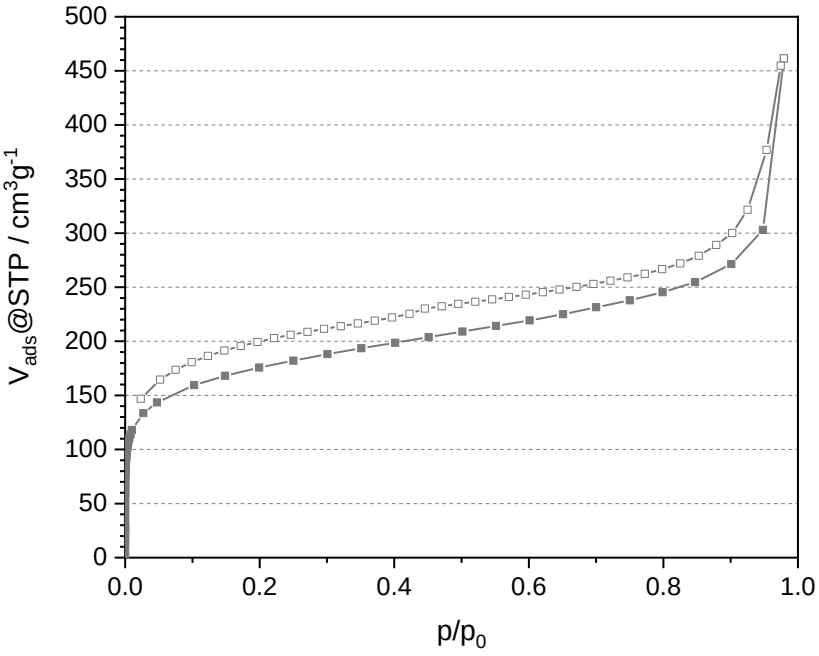

Fig. S1. Nitrogen physisorption isotherm (at 77 K) for PP-1.

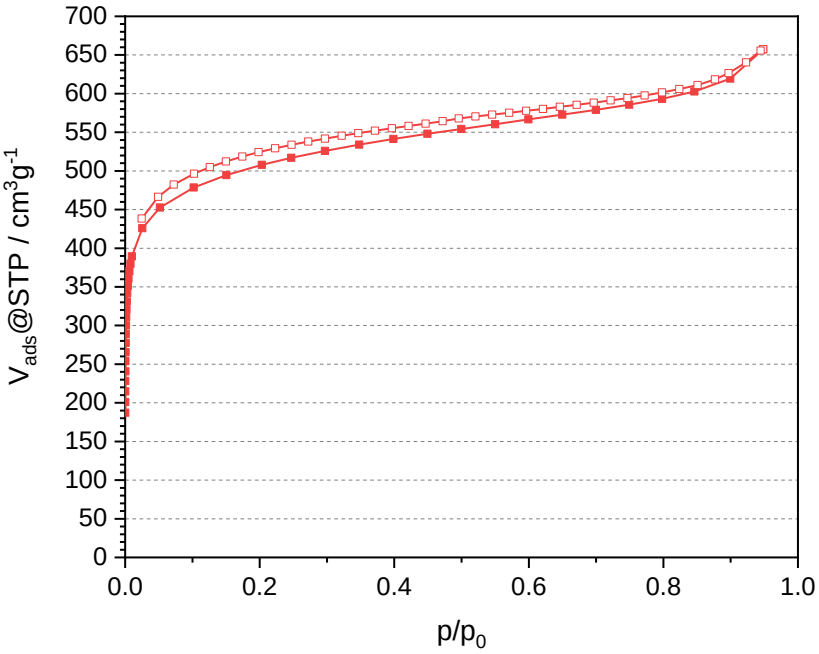

Fig. S2. Nitrogen physisorption isotherm (at 77 K) for PP-2.

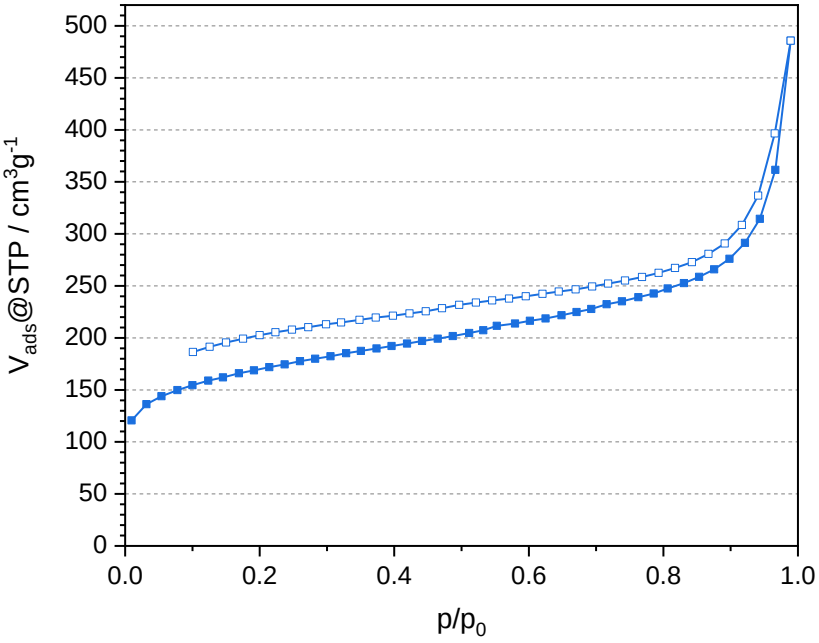

Fig. S3. Nitrogen physisorption isotherm (at 77 K) for PP-3.

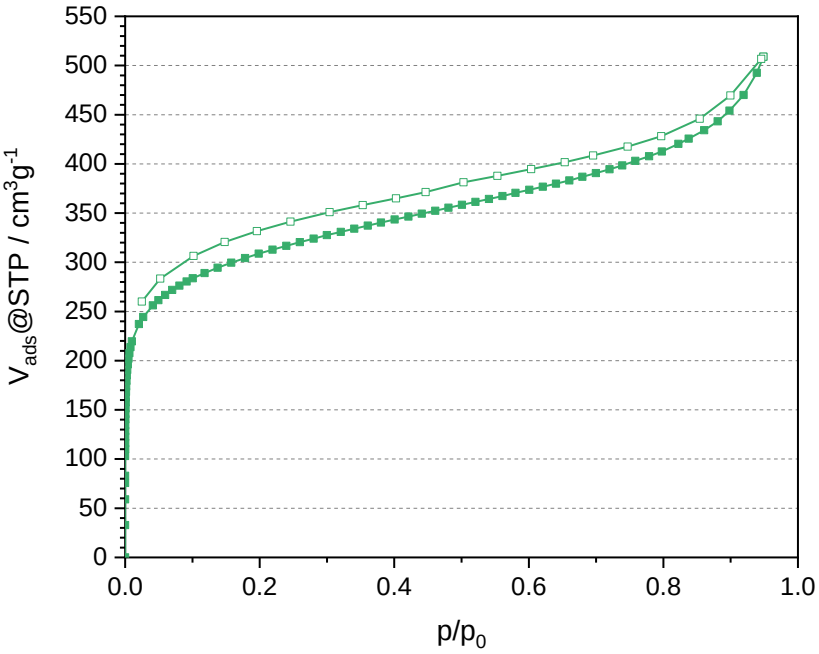

Fig. S4. Nitrogen physisorption isotherm (at 77 K) for PP-4.

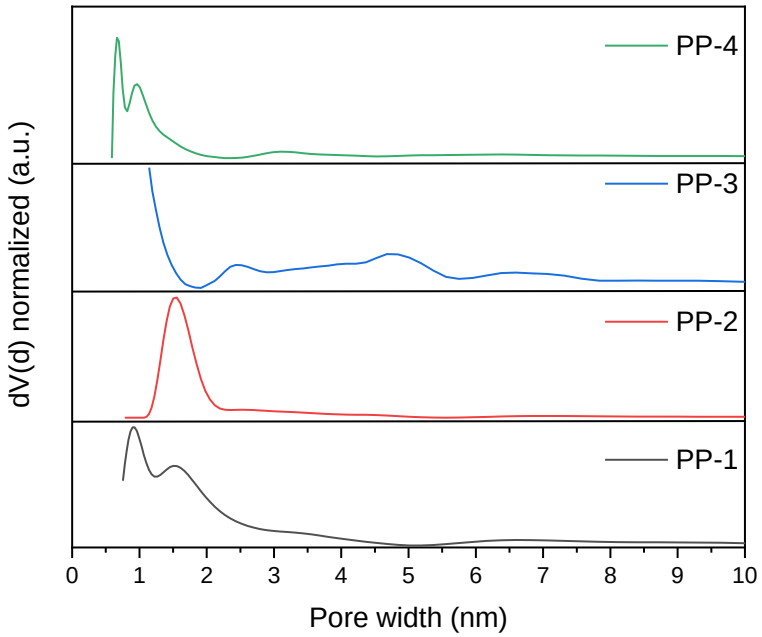

Fig. S5. Pore size distribution calculated form the isotherms S1-S4.

3.2 General characterization data for the different polymers

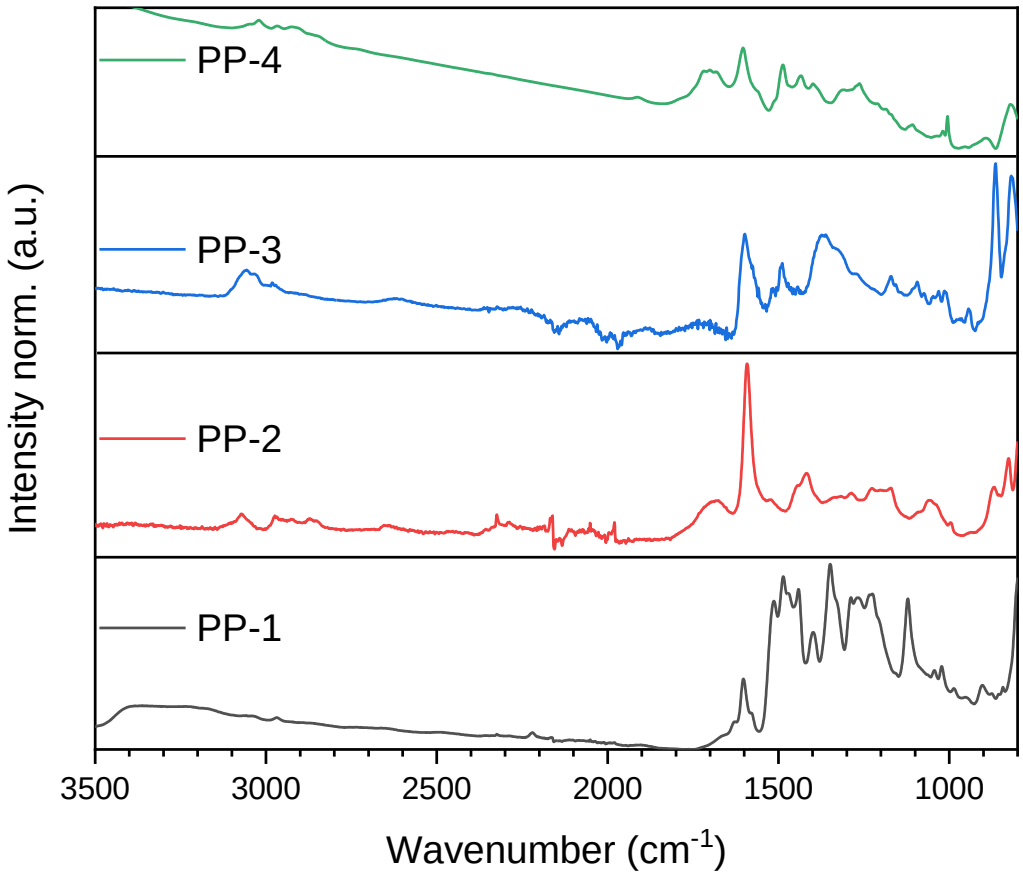

Fig. S6. FT-IR Spectra of the different polymers measured via ATR.

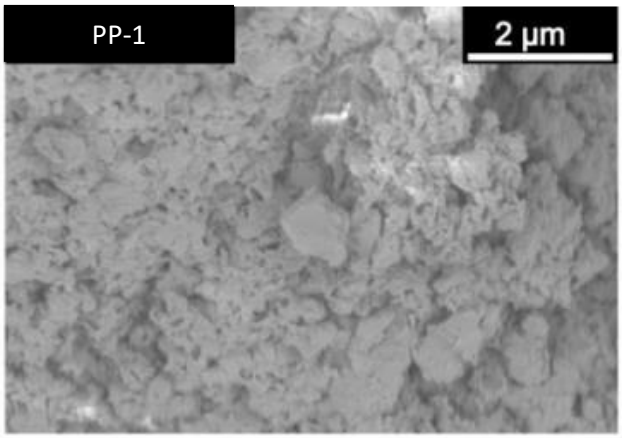

Fig. S7. SEM Picture of PP-1.

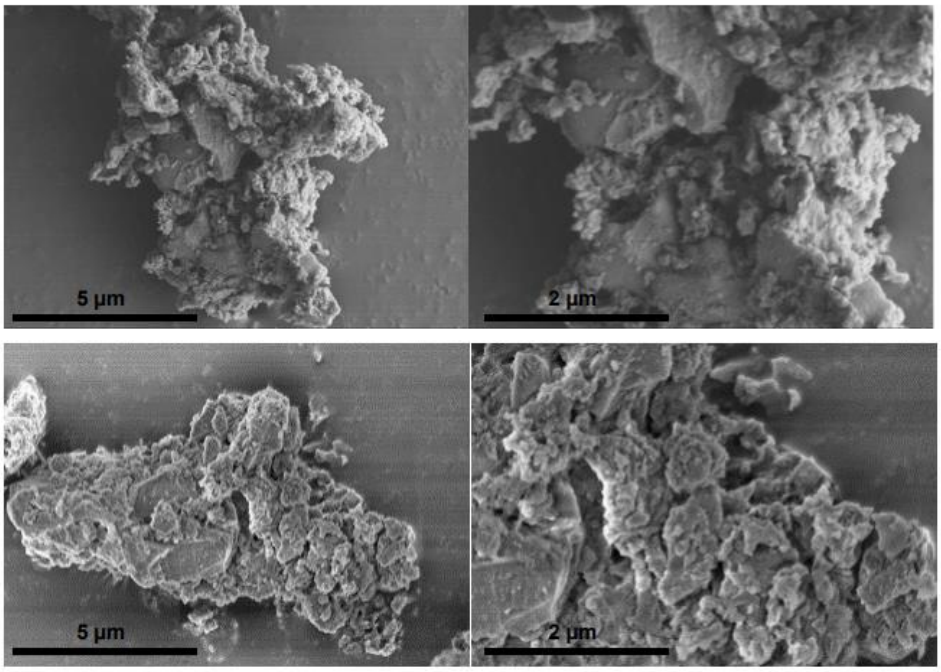

Fig. S8. SEM Picture of two different particles at two different magnifications of PP-2.

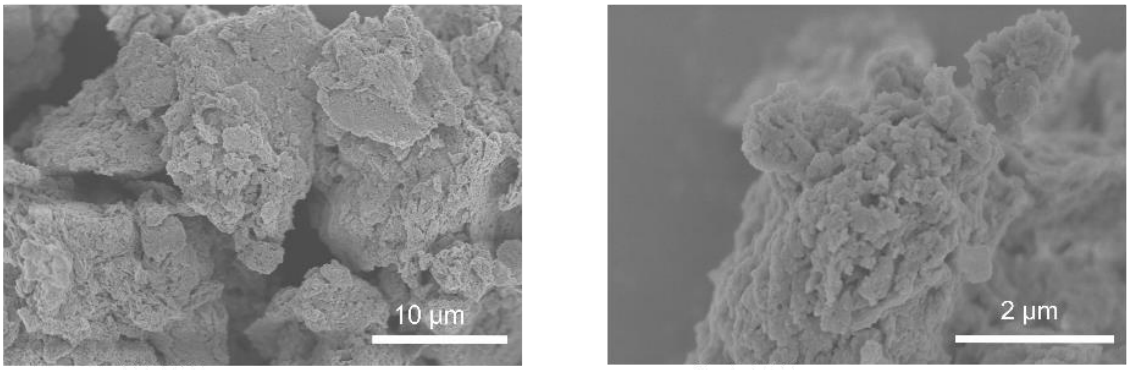

Fig. S9. SEM pictures of PP-3 at two different magnifications.

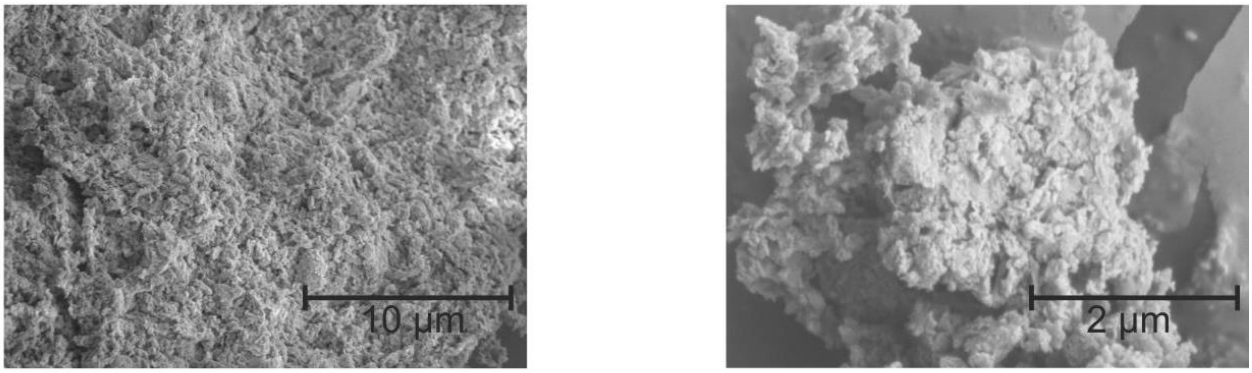

Fig. S10. SEM images of PP-4 at two different magnifications.

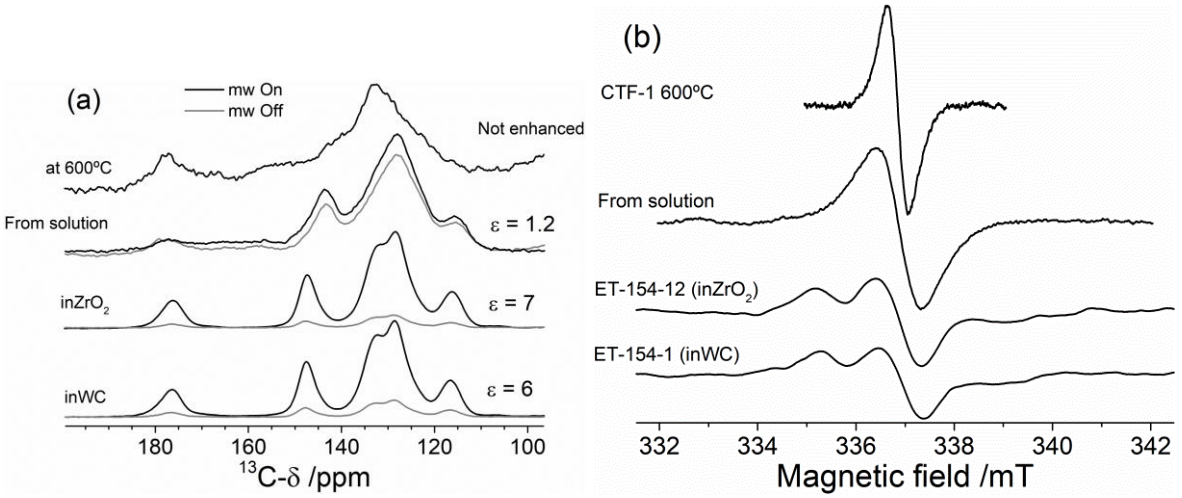

Fig. S11. (a) $^{13}C\{^{1}H\}$ CP NMR NMR spectra for compound PP-1 obtained by different synthetic routes, namely melt-polymerization at 600°C, solution-based polymerization and mechanochemical polymerization with zirconium dioxide or tungsten carbide as milling materials. Black curves in (a) represent data obtained with microwave irradiation, while grey curves represent data obtained without mw irradiation. The DNP enhancements (ε) measured for each sample are expressed within the plot. (b) Continuous-wave EPR spectra for the investigated compounds. The data is normalized by the area of the integrated spectra. For the samples prepared with WC and with ZrO_2 balls, respectively, the EPR spectra show a hyperfine profile compatible with coupling with ^{14}N species (g_{xx} = 2.0059, g_{yy} = 2.0021 and g_{zz} = 2.0010; $A_{\parallel}$ = 52.5 MHz and $A_{\perp}$= 2.8 MHz). The spectra for the samples prepared in solution and at 600 ºC show narrow isotropic lines and the hyperfine-splitting is not resolved. The narrowing occurs most probably due to the electron-electron exchange interaction. Therefore, we conclude that for these two samples the concentration of radicals is higher than for the previously measured ones. The concentration of paramagnetic radicals is the highest for the CTF sample, as shown by the extremely narrowed spectrum.

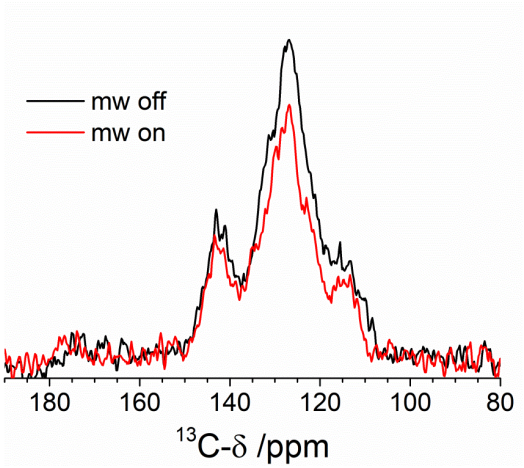

Figure S12: $^{13}C\{^{1}H\}$ CP MAS NMR spectra for the dry (without addition of polarizing solvents) PP-1 compound measured at low temperature with (black curves) and without (grey curves) mw irradiation. There is no DNP enhancement. The spectrum measured with mw irradiation has lower intensity due to heating of the sample.

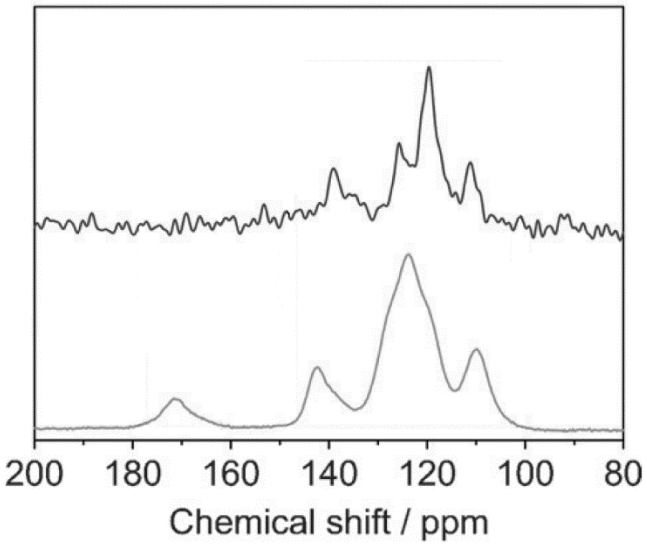

Figure S13: $^{13}C\{^{1}H\}$ CP MAS NMR of PP1 by conentional methodes published in [6]. The top sepctrum is the one of the monomer carbazole and the bottom spectrum the polymer.

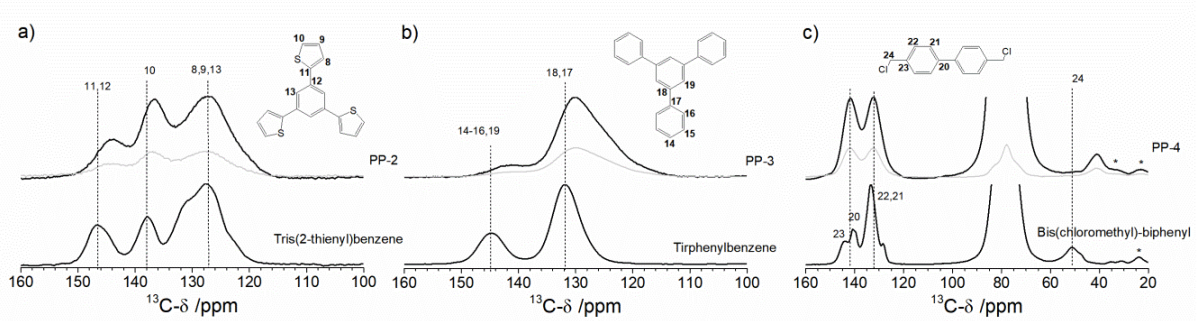

Figure S14: $^{13}C\{^{1}H\}$ CP MAS NMR spectra for the PP-2 (a), PP-3(b) and PP-4 (c) polymers (top spectra) measured with (black curves) and without (grey curves) mw irradiation. The spectra for the monomeric precursors are also shown (bottom spectra). Numbers on the top of the lines represent attributions of the lines to the carbon species observed for the molecules of the precursors (schemes shown as insets). Asterisks indicate spinning sideband positions. The signal around 76 ppm, with an extrapolated intensity, corresponds to the carbons in the TCE matrix used in the experiments. DNP enhancements of $\varepsilon = 3 \pm 1$ were obtained for all polymers, as calculated from the ratio of the spectral area with and without mw irradiation. Note that the TCE signal was excluded from this analysis.

References

1 M. Thommes, K. Kaneko, A. V. Neimark, J. P. Olivier, F. Rodriguez-Reinoso, J. Rouquerol and K. S.W. Sing, *Pure Appl. Chem.*, 2015, **87**, 1051–1069.

2 A. Zagdoun, G. Casano, O. Ouari, M. Schwarzwälder, A. J. Rossini, F. Aussenac, M. Yulikov, G. Jeschke, C. Copéret, A. Lesage, P. Tordo and L. Emsley, *J. Am. Chem. Soc.*, 2013, **135**, 12790–12797.

3 S. Y. Liao, M. Lee, T. Wang, I. V. Sergeyev and M. Hong, *Journal of biomolecular NMR*, 2016, **64**, 223–237.

4 L. Lumata, S. J. Ratnakar, A. Jindal, M. Merritt, A. Comment, C. Malloy, A. D. Sherry and Z. Kovacs, *Chem. Eur. J.*, 2011, **17**, 10825–10827.

5 T. Kobayashi, O. Lafon, A. S. L. Thankamony, I. I. Slowing, K. Kandel, D. Carnevale, V. Vitzthum, H. Vezin, J.-P. Amoureux, G. Bodenhausen and M. Pruski, *Phys Chem Chem Phys*, 2013, **15**, 5553–5562.

6 E. Troschke, S. Grätz, T. Lübken and L. Borchardt, *Angew. Chem.*, 2017, **129**, 6963–6967.

7 A. Krusenbaum, S. Grätz, S. Bimmermann, S. Hutsch and L. Borchardt, *RSC Adv.*, 2020, **10**, 25509–25516.

8 S. Grätz, S. Zink, H. Kraffczyk, M. Rose and L. Borchardt, *Beilstein J. Org. Chem.*, 2019, **15**, 1154–1161.

9 S. Grätz, M. Oltermann, E. Troschke, S. Paasch, S. Krause, E. Brunner and L. Borchardt, *J. Mat. Chem. A*, 2018, **6**, 21901–21905.